Accepted Manuscript

Low GWP refrigerants R1234ze(E) and R1234ze(Z) for high temperature heat pumps

Sho Fukuda, Chieko Kondou, Nobuo Takata, Shigeru Koyama

PII: S0140-7007(13)00292-2

DOI: 10.1016/j.ijrefrig.2013.10.014

Reference: JIJR 2665

To appear in: *International Journal of Refrigeration*

Received Date: 10 July 2013

Revised Date: 2 October 2013

Accepted Date: 31 October 2013

Please cite this article as: Fukuda, S., Kondou, C., Takata, N., Koyama, S., Low GWP refrigerants R1234ze(E) and R1234ze(Z) for high temperature heat pumps, *International Journal of Refrigeration* (2013), doi: 10.1016/j.ijrefrig.2013.10.014.

Title:

Low GWP refrigerants R1234ze(E) and R1234ze(Z) for high temperature heat pumps

Authors:

Sho Fukuda[1], Chieko Kondou*[1], Nobuo Takata[1], Shigeru Koyama[1, 2]

Affiliations:

1, Interdisciplinary Graduate School of Engineering Sciences, Kyushu University, 6-1 Kasuga-koen, Kasuga, Fukuoka 816-8580, Japan

2, International Institute for Carbon-Neutral Energy Research (WPI-I2CNER), Kyushu University, 6-1 Kasuga-koen, Kasuga, Fukuoka 816-8580, Japan

* Corresponding author.

Tel.: +81 92 583 7832

Fax: +81 92 583 7833

E-mail address: kondo.chieko.162@m.kyushu-u.ac.jp (C. Kondou)

ABSTRACT

Low global warming potential refrigerants R1234ze(E) and R1234ze(Z) are anticipated to be the refrigerants of choice for high-temperature heat pump systems in industrial applications. Their thermodynamic attributes are thermodynamically, experimentally, and numerically assessed in this study. The thermodynamic assessment indicates that the theoretical coefficients of performances (COP) are maximized at a condensation temperature approximately 20 K below the critical temperatures for each refrigerant. However, when the volumetric capacity is inadequate, the actual COP differs from the theoretical COP because of the large pressure drop. The breakdown of irreversible losses, which are experimentally quantified at a condensation temperature of 75 °C, results in the largest portion of the total pressure drop. The simulation results obtained at condensation temperatures of 105 and 125 °C indicate higher COPs than that at 75 °C for R1234ze(Z). The major factor is the reduction in the irreversible loss caused by the pressure drop. The above assessments demonstrate that R1234ze(Z) is suitable for high-temperature applications rather than in typical air conditioners.

Keywards;

low GWP, R1234ze(E), R1234ze(Z), high-temperature heat pump, irreversible loss

NOMENCLATURE

COP	coefficient of performance,	-
C_p	isobaric heat capacity,	J kg^{-1} K^{-1}
L	irreversible loss,	W
P	pressure,	Pa

Q	heat transfer rate and heating load,	W
T	temperature,	K
U	uncertainty	
V	volumetric flow rate,	$m^3 s^{-1}$
$VC_{heating}$	volumetric capacity for heating,	$J\ m^{-3}$
W_{COMP}	energy required for compression,	W
h	specific enthalpy,	$J\ kg^{-1}$
m	mass flow rate,	$kg\ s^{-1}$
s	entropy,	$J\ kg^{-1}K^{-1}$
η	compressor efficiency,	-
ρ	density,	$kg\ m^{-3}$

Subscripts

COMP	compressor
EVA	evaporator
COND	condenser
EXP	expansion valve
H2O	water
ref	refrigerant
ΔP	pressure drop
in	inlet

out	outlet
ideal	ideal cycle without pressure drop
total	total
isentro	isentropic process
th	theoretical

Superscripts

n	number of partitions in simulation

1. Introduction

R1234ze(E) and the isomer R1234ze(Z) are potential refrigerants for high-temperature heat pumps that work as hot dryers and steam generators for industrial purposes, such as concentration of beverages, sterilization of foods, drying lumber, solvent recovery, and distillation of petrochemical products. For these industrial applications, heat pumps are capable of increasing the temperature of the waste-heat source to a higher, more useful temperature (Kew, 1982). Therefore, replacing conventional combustion systems and electric heaters with heat pump systems can facilitate fuel savings and reduce CO_2 emissions. However, the global warming potentials (GWP) of some refrigerants used in such heat pump systems are high. For instance, the GWP_{100} of R245fa, which is a widely used as a working fluid in organic Rankine cycles and industrial heat pumps, is 1030. Very recently, R1234ze(Z) was nominated as an alternative to R245fa due to its very similar thermodynamic properties and extremely low GWP (GWP_{100} < 10). Similarly, R1234ze(E), with a GWP_{100} of 6, has been nominated as an alternative for R134a (GWP_{100} = 1430). The advantage of applying these refrigerants is that the production of R1234ze(E) yields the byproduct of the isomer R1234ze(Z). Meanwhile, DR-2 was considered to be an R245fa alternative by Kontomaris (2012), and the discussion of this low-GWP refrigerant for high-temperature applications is currently still controversial.

Bertinat (1985) reported a comparative assessment of 250 potential refrigerants for high-temperature heat pump condensing at 150 °C. In his report, it was proposed that the most important factors for screening refrigerants is COP, a specific compressor displacement (SCD), which is the inverse of the volumetric capacity, and the minimum superheat required to prevent liquid compression.

The critical temperatures of those low GWP refrigerants are so high that those refrigerants can operate sub-critical cycles under high-temperature conditions, which is often required in many industries. The possibility of introducing R1234ze(E) and R1234ze(Z) into high-temperature heat pump systems is investigated in this study. In a preliminary

assessment, the cycle performances of these refrigerants are thermodynamically analyzed. Then, R1234ze(E) and R1234ze(Z) are experimentally examined in a laboratory apparatus using an existing compressor developed for R410A. Additionally, the irreversible losses were numerically quantified to compare their thermodynamic attributes for high-temperature applications.

2. Thermodynamic assessments of R1234ze(E) and R1234ze(Z)

Table 1 compares the fundamental characteristics of R1234ze(E), R1234ze(Z), and selected existing refrigerants. According to the investigation by Osafune et al. (2013) and Koyama et al. (2012, 2013), R1234ze(Z) is expected to be categorized as ASHRAE safety classification A2L, and most metals, plastics, and elastomers are stable in this refrigerant. The physical properties are calculated using Refprop ver. 9 (Lemmon et al., 2010) coupled with the incorporated coefficients optimized by Akasaka et al. (2013) from the measurement data provided by Higashi et al. (2013) and Kayukawa et al. (2012). To assess the thermodynamic attributes of R1234ze(E), R1234ze(Z), and other selected refrigerants for high-temperature applications, the critical factors for refrigerant screening proposed by Bertinat (1985), the COP, the volumetric capacity, and the minimum superheat, are compared. Among these factors, the minimum superheat is irrelevant for the selected refrigerants. Thus, the remaining factors are evaluated under the following conditions.

2.1 Calculation conditions

Table 2 lists the calculation conditions. A theoretical COP of an ideal reversed Rankine cycle and a volumetric capacity for heating are evaluated at various condensation temperatures above 30 °C. The COP is calculated under the following assumptions: refrigerants are condensed and evaporated in an isobaric process, expanded in an isenthalpic process, and

compressed in an isentropic process without a clearance volume or leakage. The difference between the condensation temperature and the evaporation temperature is constantly fixed at 35 K. Similarly, the degree of subcool in the condenser and the degree of superheat in the evaporator are fixed at 20 and 3 K, respectively, corresponding to the results of the drop-in experiments, as will be discussed later in Section 3. The theoretical COP, COP_{th}, is defined as

$$COP_{th} = \frac{h_{COND,in} - h_{COND,out}}{W_{COMP,isentro}} \quad (1)$$

where $h_{COND,in}$ is the enthalpy at the condenser inlet determined by the superheat of 3 K and the isentropic curve. $h_{COND,out}$ is the enthalpy at the condenser outlet, referring to the subcool of 20 K. $W_{COMP,isentro}$ is the compression work assuming an isentropic compression process.

A volumetric heating capacity, $VC_{heating}$, indicates the heating capacity including the de-superheating and subcooling per unit mass of circulating refrigerant divided by the specific volume of the vapor at the compressor suction valve (Domanski et al., 1992). This is defined as

$$VC_{heating} = \left(h_{COND,in} - h_{COND,out}\right) \times \rho_{COMP,in} \quad (2)$$

where $\rho_{COMP,in}$ is the density of the compressor suction vapor, referring to the superheat of 3 K.

2.2 Calculation results for the theoretical COP and volumetric capacity

Figure 1 shows the calculated theoretical COPs and the volumetric capacities of the ideal reversed Rankine cycle for R1234ze(E), R1234ze(Z), R410A, R134a, and R245fa. Each refrigerant has a particular condensation temperature that maximizes the COP, approximately 20 K below the critical temperature. That is almost identical to the results found by McLinden (1988) in which it was concluded that the reduced condensation temperature yields a high COP was approximately 0.7. The COP of R410A was the lowest among the selected refrigerants, while the volumetric capacity of R410A is the largest at condensation temperatures up to 71 °C. At the same condensation temperature, the COP of

R1234ze(Z) is larger than that of R1234ze(E). The volumetric capacity of R1234ze(Z) is, however, lower than that of R1234ze(E). When the volumetric capacity is remarkably small, as indicated by a large pressure drop, there is the concern that the COP is significantly lower than the theoretical value (McLinden, 1990; Domanski and McLinden, 1992). To avoid this problem, a larger unit is required. For instance, to maintain the cooling/heating capacity, the compressor displacement volume must be increased in order to increase the circulating mass flow rate of refrigerant. With an increased circulation mass flow rate of a less-dense refrigerant vapor, the pressure drop can increase drastically. Thus, the diameters of the connection pipes and thermal tubes in heat exchangers should be enlarged to reduce the pressure drop. Otherwise, the actual COP can be drastically lower than the estimated COP as a result of the large pressure drop and the decrease in the compressor efficiency. As mentioned above, it should be noted that this thermodynamic assessment may not be appropriate or realistic when the volumetric capacity is insufficient. For R1234ze(E) and R1234ze(Z), the volumetric capacities achieve 8 MJ m^{-3} at condensation temperatures of 88 °C and 125 °C, and the COPs are maximized at 92 °C and 130 °C, respectively. Thus, this assessment suggests that the condensation temperatures at which R1234ze(E) and R1234ze(Z) deliver the best performances are approximately 90 °C and 130 °C, respectively.

3. More practical assessments considering irreversible losses

3.1 Experimental apparatus

Figure 2 is a schematic diagram of an experimental apparatus used for an experimental assessment, the “drop-in test”. The experimental apparatus consists of a refrigerant loop, a heat sink water loop, and a heat source water loop. The refrigerant loop is composed of an inverter-controlled compressor (1), an oil separator (2), a double-tube-type condenser (3), a solenoid expansion valve (4), and a double-tube-type evaporator (5). Using thermostatic baths (6), the

heat sink water and heat source water are supplied to the condenser and the evaporator. Four mixing chambers are installed between the main components in the refrigerant loop in order to measure the refrigerant pressure and the bulk-mean temperature. The refrigerants' specific enthalpies in the mixing chambers are determined from those two intensive variables. The other four mixing chambers are installed in the heat sink and heat source water loops in order to measure the bulk-mean water temperatures at the inlet and outlet of the condenser and the evaporator. In the condenser and the evaporator, the refrigerant flows inside of the inner tube, while the heat sink/heat source water flows in the annulus surrounding the inner tube.

3.2 Experimental conditions

Table 3 lists the experimental conditions of the drop-in test performed for high-temperature applications. Over the entire range of test conditions, the degree of superheat at the evaporator outlet is constantly adjusted to 3 K. The temperatures of the heat sink water and heat source water are also fixed as follows: the heat sink water temperatures at the inlet and outlet of the condenser are held at 50 °C and 75 °C, respectively, and the heat source water temperatures at the inlet and the outlet of the evaporator are held at 45 °C and 39 °C, respectively. Additionally, the heating load ranged from 1.2 kW to 2.4 kW depending on the type of refrigerant used. The amount of refrigerant charge is also varied as one of the experimental parameters in order to maintain the pressure ratio of the compressor discharge to suction below 6. Then, the optimum charge amount that maximizes the COP is found. With the optimum charge amount, the degree of subcool of the refrigerants typically ranges from 20 to 25 °C. The isentropic efficiency of the compressor ranged from 0.71 to 0.84. In addition, the heat loss in the discharge line, including the oil separator, and the pressure loss in the suction line around the compressor were considerably large and were necessarily taken into account

in the evaluation of cycle performance. The heat loss ranged from 0.09 to 0.12 kW, and the length of the suction line was approximately 3 m.

3.3 Calculation conditions for simple simulations

A similar experimental case is numerically simulated. Following the experimental conditions, the parameters of the simulation are given as listed in Table 3. The heating load Q_{COND}, the isentropic efficiency $\eta_{isentro}$, and the heat loss in the discharge line Q_{loss} are determined to be 1.8 kW, 0.74, and 0.1 W, respectively. In addition to the case, similar to the experimental conditions, the conditions at higher condensation temperatures are simulated beyond the limit of experimental assessment. Under the conditions of "simulation I" and "simulation II", the temperatures of the heat sink water in the condenser are given as 75 (in) / 100 (out) °C and 95 (in) / 120 (out) °C, respectively, while the temperatures of the heat source water in the evaporator are given as 70 (in) /64 (out) °C and 90 (in) / 84 (out) °C, respectively.

Table 4 lists the correlations applied for the simulation. With those correlations, the pressure and mass flow rate of the refrigerant are iteratively calculated until the total heat transfer rates in the condenser and the evaporator balance within 0.5% between the water side and the refrigerant side.

3.4 Data Reduction

The heat transfer rates in the condenser and evaporator are calculated from the water-side heat balance. When the refrigerant flow at the condenser inlet is superheated, the heat transfer rate can be calculated also from the refrigerant-side heat balance as follows:

$$Q_{COND} = V_{H2O}\rho_{H2O}Cp_{H2O}\left(T_{H2O,COND,out} - T_{H2O,COND,in}\right) - Q_{loss} = m_{ref}\left(h_{COND,in} - h_{COND,out}\right) \quad (3)$$

$$Q_{\mathrm{EVA}} = V_{\mathrm{H2O}}\rho_{\mathrm{H2O}}Cp_{\mathrm{H2O}}\left(T_{\mathrm{H2O,COND,out}} - T_{\mathrm{H2O,COND,in}}\right) + Q_{\mathrm{loss}} = m_{\mathrm{ref}}\left(h_{\mathrm{EVA,in}} - h_{\mathrm{EVA,out}}\right) \tag{4}$$

where Q is the heat transfer rate. V_{H2O}, ρ_{H2O}, Cp_{H2O}, and T_{H2O} are the volumetric flow rate, density, heat capacity, and bulk mean temperature of the water. m_{ref} is the mass flow rate of the refrigerant, and h is the enthalpy. The subscripts COND and EVA indicate the condenser and the evaporator, respectively. The subscripts "in" and "out" indicate the inlet and the outlet, respectively. The heat transfer rate in the condenser Q_{COND} corresponds to the heating load. The propagated measurement uncertainties were 1.5% and 2.5% for the heat transfer rates Q_{COND} and Q_{EVA}, respectively.

The COP is obtained from the heating load Q_{COND} and the compression work W_{COMP}.

$$COP = \frac{Q_{\mathrm{COND}}}{W_{\mathrm{COMP}}} = \frac{V_{\mathrm{H2O}}\rho_{\mathrm{H2O}}Cp_{\mathrm{H2O}}\left(T_{\mathrm{H2O,COND,out}} - T_{\mathrm{H2O,COND,in}}\right) - Q_{\mathrm{loss}}}{m_{\mathrm{ref}}\left(h_{\mathrm{COMP,out}} - h_{\mathrm{COMP,in}}\right)} \tag{5a}$$

$$COP' = \frac{\left(h_{\mathrm{COND,in}} - h_{\mathrm{COND,out}}\right)}{\left(h_{\mathrm{COMP,out}} - h_{\mathrm{COMP,in}}\right)} \tag{5b}$$

The COP given by Eq. (5a) is obtained from water-side heat balance. On the other hand, COP given by Eq. (5b) is obtained from refrigerant side enthalpy balance. The calculation procedure of propagated measurement uncertainties in *COP* and *COP'* are specified in Appendix A, and the uncertainties are plotted in Figure 7.

Above mentioned COPs take into account the isentropic efficiency in the compressor, but not the mechanical, volumetric, and inverter efficiencies. Although COP is normally defined by the total compressor energy consumption, in order to focus on the assessment of refrigerant properties itself, the efficiencies specific to the tested compressor are separated from the discussion on COP in this study. The brief assessment on the compressor efficiency will be described in Appendix B. The compressor isentropic efficiency is defined as

$$\eta_{\mathrm{isentro}} = \frac{W_{\mathrm{COMP,isentro}}}{W_{\mathrm{COMP}}} = \frac{h_{\mathrm{COMP,out,isentro}} - h_{\mathrm{COMP,in}}}{h_{\mathrm{COMP,out}} - h_{\mathrm{COMP,in}}} \tag{6}$$

where $h_{\mathrm{COMP,out,isetro}}$ is the ideal compressor discharge enthalpy on the isentropic curve departing from the point that refers to the compressor suction.

$$h_{\text{COMP, out, isentro}} = f\left(P_{\text{COMP,out}}, s_{\text{COMP,in}}\right) \quad (7)$$

To evaluate the cycle performance, the irreversible loss (de'Rossi et al., 1991) was calculated as follows. The total irreversible loss during cycling is divided into the irreversible losses of the main elements (e.g., compressor, evaporator, etc.) and the pressure drop, as follows:

$$L_{\text{total}} = L_{\text{COND}} + L_{\text{EVA}} + L_{\text{EXP}} + L_{\text{COMP}} + L_{\Delta P} \quad (8)$$

Figure 3 (a) illustrates the irreversible losses generated in the main components on a T-s diagram. The irreversible losses are calculated for four components: the condenser, the evaporator, the expansion valve, and the compressor. From the measured data, the temperature and the specific entropy are calculated by assuming that the specific enthalpy changes in the heat exchangers are proportional to the pressure. Specifically, the relation between pressure and enthalpy is linearly interpolated from the inlet and outlet quantities of state given by the measured parameters. With the interpolated pressure and enthalpy, the temperature and entropy in heat exchangers are determined. This simplification may be justified because the temperature change due to the estimation error in pressure should be subtle, relative to the temperature difference between water and refrigerant. The irreversible losses in each component are quantified as follows:

$$L_{\text{COND}} = m_{\text{ref}} \times \sum_{n}\left[\left(T_{\text{ref}}^{n} - T_{\text{H2O}}^{n}\right) + \left(T_{\text{ref}}^{n+1} - T_{\text{H2O}}^{n+1}\right)\right]\Delta s^{n} \Big/ 2 \quad (9)$$

$$L_{\text{EVA}} = m_{\text{ref}} \times \sum_{n}\left[\left(T_{\text{H2O}}^{n} - T_{\text{ref}}^{n}\right) + \left(T_{\text{H2O}}^{n+1} - T_{\text{ref}}^{n+1}\right)\right]\Delta s^{n} \Big/ 2 \quad (10)$$

$$L_{\text{EXP}} = m_{\text{ref}} \times \left(T_{\text{ref,EXP,in}} + T_{\text{ref,EXP,out}}\right)\left(s_{\text{ref,EXP,out}} - s_{\text{ref,EXP,in}}\right)/2 \quad (11)$$

$$L_{\text{COMP}} = m_{\text{ref}} \times \left(T_{\text{ref,COMP,in}} + T_{\text{ref,COMP,out}}\right)\left(s_{\text{ref,COMP,out}} - s_{\text{ref,COMP,in}}\right)/2 \quad (12)$$

where L is the irreversible loss, T_{ref} and T_{H2O} are temperatures of the refrigerant and water, respectively, and Δs is the specific entropy change through the components or a segment. Subscripts COND, EVA, EXP, and COMP indicate the condenser, the evaporator, the expansion valve, and the compressor, respectively. For the quantification of L_{cond} and

L_{EVA} from the experimental results, the hatched areas shown in Figure 3 (a) were equally partitioned into 100 segments in the direction of entropy, assuming that the water temperature changes proportionally to the entropy change of the refrigerant. For the simple simulation, the area refers to the irreversible losses, and L_{cond} and L_{EVA} are unequally partitioned into 40 segments. The distribution of the unequal segments was arbitrarily determined in order to reduce the calculation error, and the temperature distributions through the condenser and evaporator are calculated for each segment.

Figure 3 (b) illustrates the irreversible loss caused by the pressure drop $L_{\Delta P}$. This irreversible loss $L_{\Delta P}$ is obtained as the difference of the actual cycle from the ideal cycle assuming no pressure drop. In Figure 3 (b), the dashed line shows the ideal cycle obtained from only the enthalpy change, eliminating the effect of the pressure drop. The hatched areas framed by the dashed and solid lines indicate the irreversible loss from the pressure drop; however, it should be noted that the area $L_{\Delta P,EVA}$ is considered to be negative.

$$
\begin{aligned}
&L_{\Delta P} = L_{\Delta P,COND} + L_{\Delta P,EVA} + L_{\Delta P,EXP} + L_{\Delta P,COMP} \\
&\begin{cases}
L_{\Delta P,COND} = m_{ref} \times \sum_n \left[\left(s_{ref}^{n+1} - s_{ref,ideal}^{n} \right) \left(T_{ref}^{n} - T_{ref,ideal}^{n+1} \right) + \left(s_{ref}^{n} - s_{ref,ideal}^{n+1} \right) \left(T_{ref,ideal}^{n} - T_{ref}^{n+1} \right) \right] / 2 \\
L_{\Delta P,EVA} = m_{ref} \times \sum_n \left[\left(s_{ref}^{n+1} - s_{ref,ideal}^{n} \right) \left(T_{ref}^{n} - T_{ref,ideal}^{n+1} \right) + \left(s_{ref}^{n} - s_{ref,ideal}^{n+1} \right) \left(T_{ref,ideal}^{n} - T_{ref}^{n+1} \right) \right] / 2 \\
L_{\Delta P,EXP} = m_{ref} \times \left(T_{ref,EXP,in} + T_{ref,EXP,in,ideal} \right) \left(s_{ref,EXP,in} - s_{ref,EXP,in,ideal} \right) / 2 \\
L_{\Delta P,COMP} = m_{ref} \times \left(T_{ref,COMP,in} + T_{ref,COMP,in,ideal} \right) \left(s_{ref,COMP,in} - s_{ref,COMP,in,ideal} \right) / 2
\end{cases}
\end{aligned}
\tag{13}
$$

The number of partitions, n, is 100 (experiment) or 40 (simulation) for the condenser and the evaporator both. If the other irreversible losses were negligible, the compression works in Eqs. (5a) and (6) is also described from the heat balance in this corollary of the tested heat pump system:

$$
\begin{aligned}
&W'_{COMP} + Q_{EVA} \approx Q_{COND} + L_{total} \\
&\therefore W'_{COMP} \approx Q_{COND} + L_{total} - Q_{EVA}
\end{aligned}
\tag{14}
$$

3.5 Results of experiment and simple simulation

3.5.1 Validation of experiment and simple simulation

Table 5 compares the experimental and simulation results for the irreversible loss and the COP at a heating load of 1.8 kW. As listed in Table 5, at a condensation temperature of 75 °C, the simulation results agree with the experimental results within 20% for the irreversible losses and 18% for the COP. These deviations should be acceptable in consideration of the simplification of the simulation method and the measurement uncertainty in the experimental method.

Figures 4 and 5 plot the experimental results and the simulation results at a heating load of 1.8 kW and a condensation temperature of approximately 75 °C on the *P*-*h* diagram and *T*-*s* diagram for R1234ze(E) and R1234ze(Z), respectively. The cross and circle symbols represent the measured and calculated points, respectively. Due to the high degree of overlap of these symbols, the methods of the experiment and the simple simulation are also validated.

Figure 6 compares the compression works obtained from the enthalpy balance of W_{COMP} and from the heat balance of the corollary by Eq. (14) W'_{COMP}. As shown in Figure 6, the ratio of W_{COMP} to W'_{COMP} ranges from 9.995 to 1.005. This result confirms that the irreversible loss defined in Eq. (8) includes all major irreversible losses, and the remaining losses should be negligibly small. Thus, the omission in the data reduction method could be justified.

3.5.2 COP and heating load for R1234ze(E) and R1234ze(Z)

Figure 7 presents the experimental results for COP and heating load at the optimum amount of refrigerant charge, where the circles and triangles represent the results obtained for R1234ze(E) and R1234ze(Z), respectively. At the condensation temperature of approximately 75 °C and a heating load above 1.5 kW, the COP of R1234ze(Z) becomes lower than that of R1234ze(E) and drastically decreases with increasing heating load. This result differs from the results of the thermodynamic assessment shown in Figure 1. The main cause of this discrepancy is that the pressure

drop increases with an increasing circulation mass flow rate of the refrigerant, as explained in Section 2.2. This means that the volumetric capacity of R1234ze(Z) is obviously insufficient under the experimental conditions in the present experimental apparatus. However, at higher temperatures where the volumetric capacity is large enough for the provided heating load, the COP of R1234ze(Z) should be as high as expected by the thermodynamic assessment because of the smaller pressure drop. Therefore, under the experimental conditions applied here, R1234ze(E) should be considered a suitable low GWP refrigerant for heat pump systems, rather than R1234ze(Z). For heat pump systems that operate at higher temperatures, R1234ze(Z) would be the more suitable refrigerant.

3.5.3 Breakdown of irreversible losses at a condensation temperature of 75 °C

Figure 8 shows the breakdown of the irreversible losses obtained from the simple simulation at a heating load of 1.8 kW for R1234ze(E) and R1234ze(Z). Each numerical value is specified in Table 5. With a given condensation temperature of 75 °C, the total irreversible losses of R1234ze(Z) are 50 W greater than that of R1234ze(E). As a result of the difference in irreversible losses, the COP of R1234ze(Z) is lower than that of R1234ze(E). The same characteristics are confirmed in the experimental results, as shown in Figure 8 and Table 5. At a condensation temperature of 75 °C, the irreversible losses of R1234ze(Z) in each component except the expansion valve are greater than those of R1234ze(E).

The irreversible loss that occurs through the condenser L_{COND} of R1234ze(Z) is somewhat greater than that of R1234ze(E). The quantity of the loss L_{COND} is determined by the pinch point (i.e., approaching temperature) that appears either at the inlet or the outlet of the condenser. Because of the temperature gradient caused by the pressure drop in the evaporator, the irreversible loss in the evaporator L_{EVA} becomes greater as a consequence of the increased temperature difference between the refrigerant and the heat source water. As shown in Figures 4 (b) and 5 (b), much

more compression work W_{COMP} is required for R1234ze(Z) compared to R1234ze(E), which is associated with the moderate incline of the isentropic curve. The irreversible loss caused by the pressure drop $L_{\Delta P}$ of R1234ze(Z) is approximately 3.5 times greater than that of R1234ze(E). In particular, the pressure drop through the suction line, where the superheated vapor flows at a high velocity, is significantly greater, as shown in Figure 5.

From the above characteristics of the irreversible loss, some possible solutions are suggested to improve the COP of R1234ze(Z) in practical situations, such as circuit designs to avoid the pinch point, reduce the temperature difference between refrigerant and water, increase the circuit number, and enlarge the tube diameters to reduce the intense pressure drop through the suction line.

3.5.4 Case study at condensation temperatures of 105 and 125 °C

Figure 8 and Table 5 also show the predicted breakdown of the irreversible losses and the COP obtained by the simple simulation at the condensation temperatures of 105 and 125 °C where, beyond an assured range, the applied compressor safely operates. The conditions of this simple simulation are specified as “simulation II” and “simulation III” in Table 3. As the temperature increases from 75 to 105 and then to 125 °C, the irreversible losses in the evaporator and the compressor, L_{EVA} and L_{COMP}, and the irreversible loss caused by pressure drop $L_{\Delta P}$ decrease, while the irreversible loss in the expansion valve L_{EXP} increases, assuming an isenthalpic process.

Figures 9 and 10 plot the calculation results for R1234ze(Z) at the condensation temperatures of 105 and 125 °C, respectively, on *P-h* and *T-s* diagrams. These diagrams exhibit the causes of the changes in the irreversible losses. Comparing Figures 5, 9, and 10, the temperature gradient of the refrigerant flow through the evaporator due to the pressure drop decreases depending on the increase in the temperature level of the heat source water. The reduction in the pressure drop also affects the whole corollary. As shown in Figure 1, the volumetric capacity increases with

increasing temperatures up to 150 °C. Thus, under the specified high-temperature conditions, the large volumetric capacity yields a reduction in the circulation mass flow rate. In addition, the denser refrigerant vapor yields a lower velocity of the vapor flow. Consequently, the pressure drop is reduced, especially in the suction line, which causes a reduction in the irreversible loss L_{DP}. The irreversible loss in the expansion valve L_{exp} moderately increases with increasing heat capacity due to throttling as the condensation temperature rises. This agrees with the summary mentioned by Domanski et al. (1995), which indicated that an increase in molar heat capacity predominantly increases the throttling losses in expansion valves. Nevertheless, in total, the irreversible loss of R1234ze(Z) decreases under high-temperature conditions.

As mentioned above, the case study indicates that the low GWP refrigerant R1234ze(Z) is capable of achieving a higher COP at condensation temperatures above 100 °C, which is more favorable for the potential conditions of industrial purposes, rather than air conditioners or refrigeration systems.

4. CONCLUSIONS

The performances of a high-temperature heat pump have been thermodynamically, experimentally, and numerically evaluated for the low GWP refrigerants R1234ze(E) and R1234ze(Z). From a thermodynamic assessment, the theoretical COPs and volumetric capacities of the ideal reversed Rankine cycle among R1234ze(E), R1234ze(Z), and three other refrigerants were compared. Under the provided temperature difference between condensation and evaporation, each refrigerant has a certain condensation temperature that maximizes the COP, approximately 20 K below the critical temperature. However, the concern is the inadequacy of this assessment method for conditions where the volumetric capacity is remarkably insufficient. This inadequacy, specifically, the discrepancy in COP between the thermodynamic assessment and the experimental assessment, was confirmed from the drop-in test at a condensation

temperature of 75 °C. Therefore, an assessment that considered the irreversible losses caused by the pressure drop and the compressor, the condenser, the expansion valve, and the evaporator was attempted. From the experimental ascertainment of the heat balance, it was confirmed that the remaining losses are all negligible compared to the major factors. The breakdown of irreversible losses indicated the necessity to take into account the pressure drop in the evaluation of the cycle performance. From the simple simulation, which agreed well with the experimental results, the irreversible losses and COPs were quantified at condensation temperatures of 105 and 125 °C for R1234ze(Z). The simulation results suggest that R1234ze(Z) achieves a higher COP at 105 and 125 °C because the losses related to the pressure drop are drastically reduced. As mentioned above, this attempt demonstrated that the low GWP refrigerants R1234ze(E) and R1234ze(Z) are capable of being a potential refrigerant in high-temperature heat pump systems for industrial purposes, rather than typical air conditioners or refrigeration systems.

ACKNOWLEDGEMENTS

The present study is sponsored by the project on the "Development of High Efficiency and Non-Freon Air Conditioning Systems" of the New Energy and Industrial Technology Development Organization (NEDO), Japan.

APPENDICES

A. Uncertainty analysis

Table A.1 lists the uncertainties in measured parameters. The propagated uncertainties are obtained as summation of the partial uncertainties (Taylor, 1982), assuming that the each measured parameters are independent and random. The calculation procedure for the maximum uncertainty in COP, which is plotted in Figure 7, is described below.

The COP obtained from the water-side heat balance is expressed as Eq. (5a). The uncertainty in the COP, U_{COP}, is

subject to the uncertainties in V_{H2O}, T_{H2O}, ρ_{H2O}, Cp_{H2O}, m_{ref}, $h_{COMP,out}$, and $h_{COMP,in}$. While, the partial uncertainties in the COP due to Q_{loss} is supposed to be negligible.

$$\begin{aligned} U_{COP} \approx & \left|\frac{\rho_{H2O} Cp_{H2O} \Delta T_{H2O,COND}}{m_{ref}\left(h_{COMP,out} - h_{COMP,in}\right)}\right| U_{V_{H2O}} + \left|\frac{V_{H2O} Cp_{H2O} \Delta T_{H2O,COND}}{m_{ref}\left(h_{COMP,out} - h_{COMP,in}\right)}\right| U_{\rho_{H2O}} \\ & + \left|\frac{V_{H2O} \rho_{H2O} \Delta T_{H2O,COND}}{m_{ref}\left(h_{COMP,out} - h_{COMP,in}\right)}\right| U_{Cp_{H2O}} + 2\left|\frac{V_{H2O} \rho_{H2O} Cp_{H2O}}{m_{ref}\left(h_{COMP,out} - h_{COMP,in}\right)}\right| U_{\Delta T_{H2O}} \\ & + \left|\frac{\rho_{H2O} Cp_{H2O} \Delta T_{H2O,COND}}{m_{ref}^{\,2}\left(h_{COMP,out} - h_{COMP,in}\right)}\right| U_{m_{ref}} + \left|\frac{\rho_{H2O} Cp_{H2O} \Delta T_{H2O,COND}}{m_{ref}\left(h_{COMP,out} - h_{COMP,in}\right)^2}\right| \left(U_{h_{COMP,out}} + U_{h_{COMP,in}}\right) \end{aligned} \quad \text{(A.1)}$$

where $\Delta T_{H2O,COND}$ is the water temperature change through the condenser,

$$\Delta T_{H2O,COND} = T_{H2O,COND,out} - T_{H2O,COND,in} \quad \text{(A.2)}$$

When the uncertainty in the property database is negligible, the uncertainty in the fluid properties, such as $U_{\rho_{H2O}}$, $U_{Cp_{H2O}}$, $U_{h_{COMP,out}}$, and $U_{h_{COMP,in}}$, can be calculated as the deviation between maximum and minimum values referring measured parameters. For instance, the uncertainty in refrigerant enthalpy is found with Refprop ver. 9.0 (Lemmon et al. 2010) as,

$$\begin{aligned} U_h &\approx \left(h_{\_max} - h_{\_min}\right)/2 \\ h_{\_max} &= \mathrm{Max}\left[h\left(P \pm U_P, T_{ref} \pm U_{T_{ref}}\right)\right] \\ h_{\_min} &= \mathrm{Min}\left[h\left(P \pm U_P, T_{ref} \pm U_{T_{ref}}\right)\right] \end{aligned} \quad \text{(A.3)}$$

Also, the uncertainty in COP obtained from the refrigerant-side heat balance by Eq. (5b) is calculated as,

$$U_{COP'} \approx \left|\frac{1}{h_{COMP,out} - h_{COMP,in}}\right| \left(U_{h_{COND,in}} + h_{COND,out}\right) + \left|\frac{h_{COND,in} - h_{COND,out}}{\left(h_{COMP,out} - h_{COMP,in}\right)^2}\right| \left(U_{h_{COMP,out}} + U_{h_{COMP,in}}\right) \quad \text{(A.4)}$$

As plotted in Figure 7, the calculated uncertainty in COP is less than 0.3 that is approximately 5% of the measured COP.

B. Compressor efficiency

The compressor used in this experiment was a hermetic twin rotary compressor (two rolling pistons) to perform two stage compression. The suction side volume of the chamber is 24 cm^3. The rotation speed ranges from 1500 to 6000

rpm with the inverter control. The lubricant oil applied in the compressor was POE VG68 for both refrigerants. In practical situations of industrial heat pumps, however, centrifugal compressors are often selected (Matsukura et al., 2012; Pearson, 2013) to reduce compression ratio in each stage. The compressor efficiency strongly depends on the compressor type and the combination of refrigerant and lubricant oil; therefore, the inherent efficiency of the particular compressor was separated from the evaluation of COP in Section 3. The efficiency of the tested compressor is here remarked for reference.

Figure B.1 (a) compares the volume ratio of actual compressor displacement to theoretical displacement for R1234ze(E) and R1234ze(Z). The actual compressor displacement volume is calculated from the refrigerant flow rate and the density. The theoretical displacement volume is calculated from the compressor speed and the chamber volume. From this ratio, it is expected that the volumetric efficiency of R1234ze(Z) is higher than that of R1234ze(E) at heating loads of 1.8 kW and 2.0 kW. As shown in Figure B.1 (b), the total compressor efficiency of R1234ze(Z) is slightly higher than that of R1234ze(E) at the heating loads of 1.8 kW and 2.0 kW because of the volumetric efficiency. On the other hand, as shown in Figure B.1 (c), the isentropic efficiency of R1234ze(Z) is marginally higher than that of R1234ze(E).

REFERENCES

ASHRAE STANDARD, Designation and safety classification of refrigerants, ANSI/ASHRAE Standard 34-2007, 2008.

Akasaka, R., Higashi, Y., Koyama, S., 2013. A fundamental equation of state for low GWP refrigerant HFO-1234ze(Z). In: Proc. 4th IIR Conference on Thermophysical Properties and Transfer Processes of Refrigerants, Delft, The Netherlands, 2013, Paper No. TP-052.

Akasaka, R., Kano, Y., Kayukawa, Y., Tanaka, K., Fujita, Y. and Higashi, Y., 2012. A thermodynamic equation of state for low-GWP refrigerant HFO-1234ze(Z) and its application to heat pump cycle analysis. In: Proc. Int. Symp. New Refrigerants and Environmental Technology 2012, Kobe, Japan, 193-197.

Bertinat, M.P., 1985. Fluids for high temperature heat pumps. Int. J. Refrig., 9, 43-50.

Brown, J. S., Zilio, C., Cavallini, A., 2009. The fluorinated olefin R-1234ze(Z) as a high-temperature heat pumping refrigerant. Int. J. Refrig., 32, 1412-1422.

Carnavos, T.C., 1980. Heat Transfer Performance of Internally Finned Tubes in Turbulent Flow. Heat Transfer Eng., 1 (4), 32-37.

Cavallini, A., DelCol, D., Mancin, S., Rossetto, L., 2009. Condensation of Pure and Near-Azeotropic Refrigerants in Microfin Tubes: a new computational procedure. Int. J. Refrig., 32, 162-174.

Domanski, P.A., 1995. Minimizing throttling losses in the refrigeration cycle. In: Proc. Int. Congr. Refrig., 19th, 4B, 766-773.

Domanski, P.A., Didion, D.A., Doyle, J.P., 1992. Evaluation of suction line-liquid line heat exchanger in the refrigeration cycle. In: Proc. Int. Refrigeration and Air Conditioning Conf., West Lafayette, IN, Paper no. 149, 131-139.

Domanski, P.A., McLinden, M.O., 1992. A simplified cycle simulation model for the performance rating of refrigerants and refrigerant mixtures. Int. J. Refrig., 15 (2), 81-88.

Goto, M., Inoue, N., Ishiwatari, N., 2001. Condensation and evaporation heat transfer of R410A inside internally grooved horizontal tubes. Int. J. Refrig., 24, 628–638

Goto, M., Inoue, N., Ishiwatari, N., 2007. Answer to comments by M.M. Awad on "Condensation and evaporation heat transfer of R410A inside internally grooved horizontal tubes". Int. J. Refrig., 30, 1467.

Higashi, Y., Hayasaka, S., and Ogiya, S., 2013. Measurements of PvT properties vapor pressures, and critical parameters for low GWP refrigerant R-1234ZE(Z). In: Proc. 4th IIR Conference on Thermophysical Properties and Transfer Processes of Refrigerants, Delft, The Netherlands, Paper No. TP-018

Honeywell Material Safety Data Sheet, 2011. MSDS Number: HFO-1234ze JPN, ver. 10, 1-10.

Jenasen, M.K., Vlakancic, A., 1999. Experimental investigation of turbulent heat transfer and fluid flow in internally finned tubes, Int. J. Heat Mass Transfer, 42, 1343-1351.

Kayukawa, Y., Tanaka, K., Kano, Y., Fujita, Y., Akasaka, R. and Higashi, Y., 2012. Experimental evaluation of the fundamental properties for low-GWP refrigerant HFO-1234ze(Z). In: Proc. Int. Symp. New Refrigerants and Environmental Technology 2012, Kobe, Japan, 231.

Kew, P.A., 1982. Heat pumps for industrial waste heat recovery – a summary of required technical and economic criteria. Heat Recovery System, 2 (3), 283-296.

Kondou, C., Hrnjak, P.S., 2012. Condensation from Superheated Vapor Flow of R744 and R410A at Subcritical Pressures in a Horizontal Smooth tube. Int. J. Heat Mass Transfer, 55, 2779-2791.

Kontomaris, K., 2012. A zero-ODP, low GWP working fluid for high temperature heating and power generation from low temperature heat: DR-2. In: Proc. JRAIA international symposium 2012, 212-216.

Koyama, S., Fukuda, S., Osafune, K., Akasaka, R., 2012. Development of low GWP refrigerants suitable for heat pump systems. In: Proc. Int. Symp. New Refrigerants and Environmental Technology 2012, Kobe, Japan, 135-140.

Koyama, S., Higashi, T., Miyara, A., Akasaka, R., 2013. Research and development of low-GWP refrigerants suitable for heat pump systems. In: JSRAE Risk Assessment of Mildly Flammable Refrigerants-2012 Progress Report, 29-34.

Kubota, A., Uchida, M., Shikazono, N., 2001. Predicting equations for evaporation pressure drop inside horizontal smooth and grooved tubes. Trans. JSRAE, 18 (4), 393-401 (in Japanese).

Lemmon, E.W., Huber, M.L., McLinden, M.O., 2010. Reference Fluid Thermodynamic and Transport Properties - REFPROP Ver. 9.0, National Institute of Standards and Technology, Boulder, CO, USA.

Matsukura, N., Okuda, S., Nagai, K., Ueda, K., 2012. Study of application of HFO-1234ze(E) to hot water centrifugal heat pump - Evaluation of low GWP refrigerant HFO-1234ze(E) in high temperature region. In: Proc. JSRAE annual conf., Sapporo, Japan, no. F124, 1-4 (in Japanese).

McLinden, M.O., 1988. Thermodynamic evaluation of refrigerants in the vapour compression cycle using reduced properties. Int. J. Refrig., 11, 134-143.

McLinden, M.O., 1990. Optimum refrigerants for non-ideal cycles: an analysis employing corresponding states. In: Proc. Int. Refrigeration and Air Conditioning Conf., 69-79.

Mori, H., Yoshida, S., Koyama, S., Miyara, A., Momoki, S., 2002. Prediction of heat transfer coefficients for refrigerants flowing in horizontal spirally grooved evaporator tubes. In: Proc. 14th JSRAE Annual Conf., 97-100, (in Japanese).

Osafune, K., Nishiguchi, Y., Okamoto, S., Sakyu, F., Koyama, S., 2013. Chemical/thermal stability of low GWP refrigerant HFO-1234ze(Z). In: Proc. 2013 JSRAE Annual Conf., Tokyo, Japan, no. E122, 119-121.

Pearson, A., 2013. R-1234ze for variable speed centrifugal chillers. In: Proc. Inst. Refrigeration, 2012-13.7, 1-16

Solomon, S., Qin, D., Manning, M., Chen, Z., Marquis, M., 2007. IPCC 2007 Annual Report 4th Climate Change 2007 - The Physical Science Basis, 210-216.

Taylor, J.T., 1982. An introduction to error analysis, second ed., University science book.

Wiegand, J.H., Baker, E.M., 1942. Transfer processes in annuli. Trans. AIChE, 38, 569-592.

de'Roosi, F., Mastrullo, R., Mazzei, P., 1991. Working fluids thermodynamic behavior for vapor compression cycles. Applied Energy, 38, 163-180.

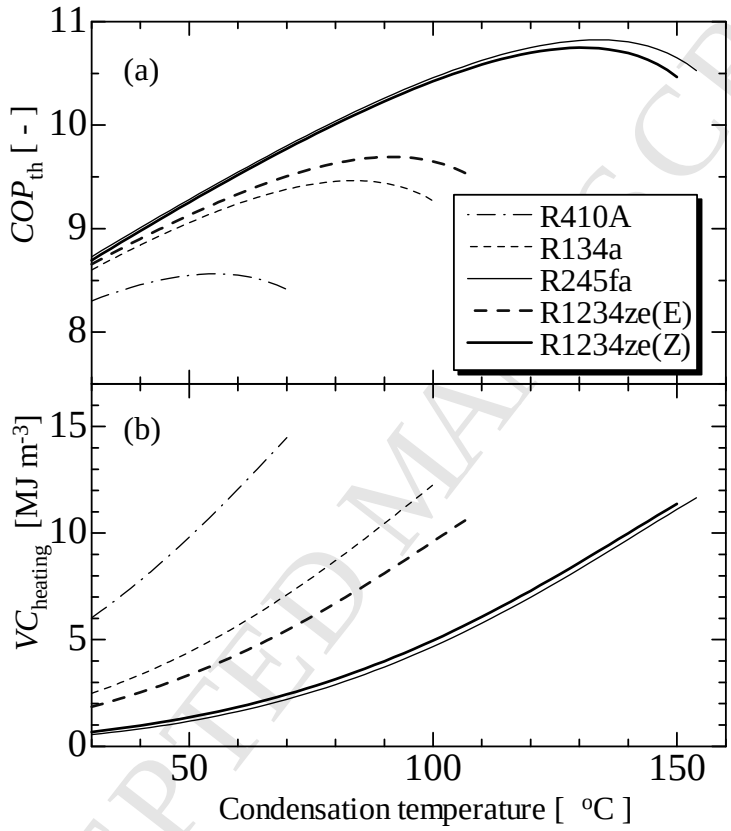

Figure 1 Results of the thermodynamic assessment assuming an ideal reversed Rankine cycle

(a) theoretical COP (b) volumetric capacity

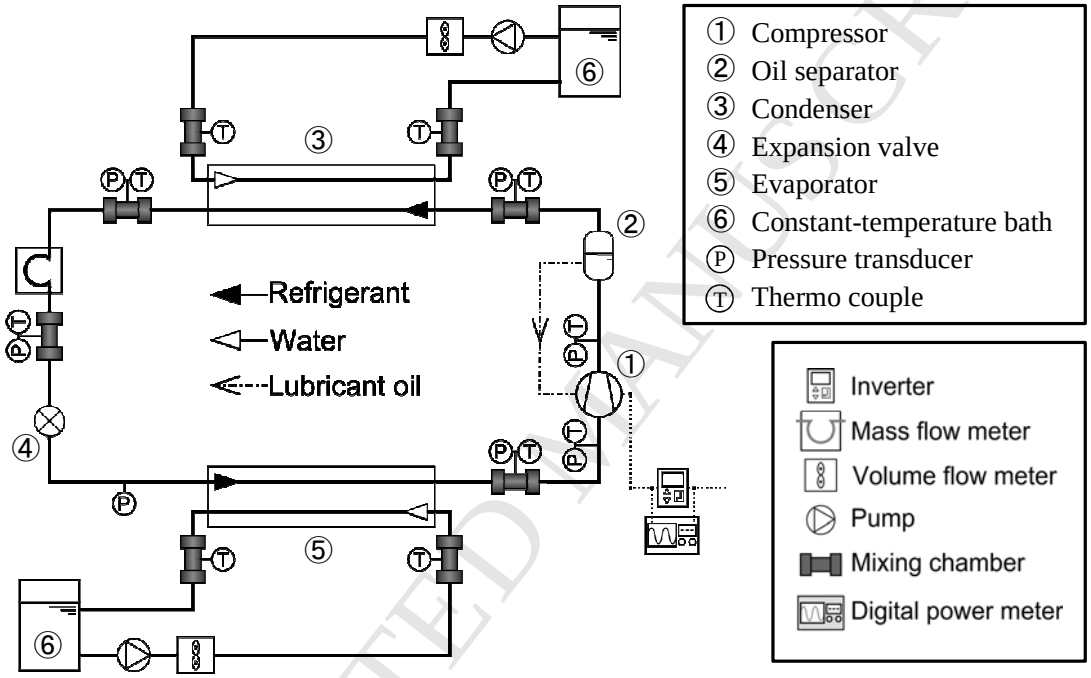

Figure 2 Experimental apparatus

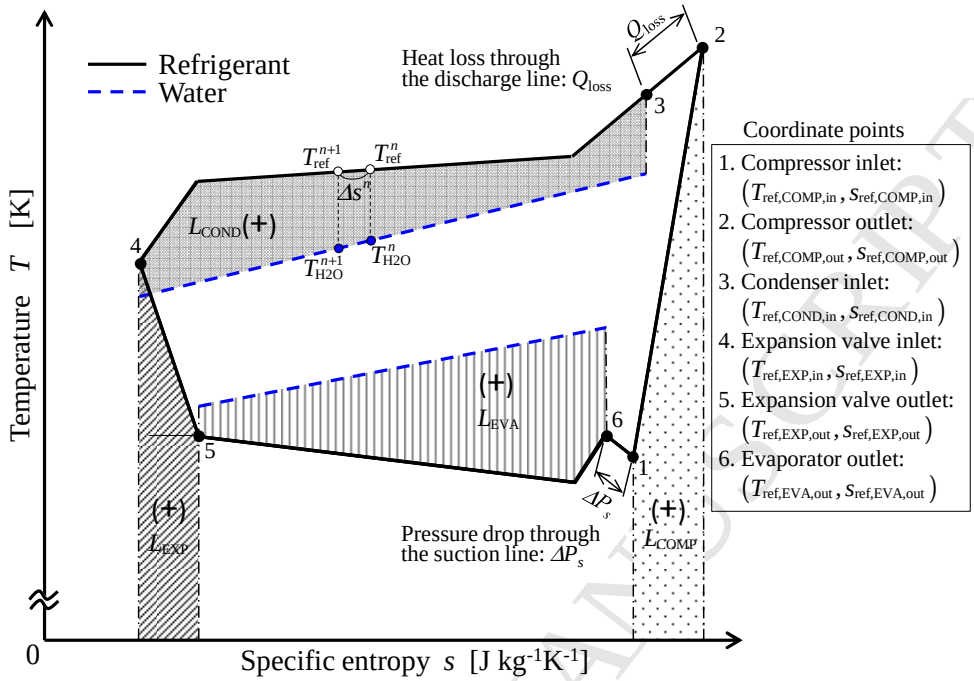

(a) irreversible losses in main components

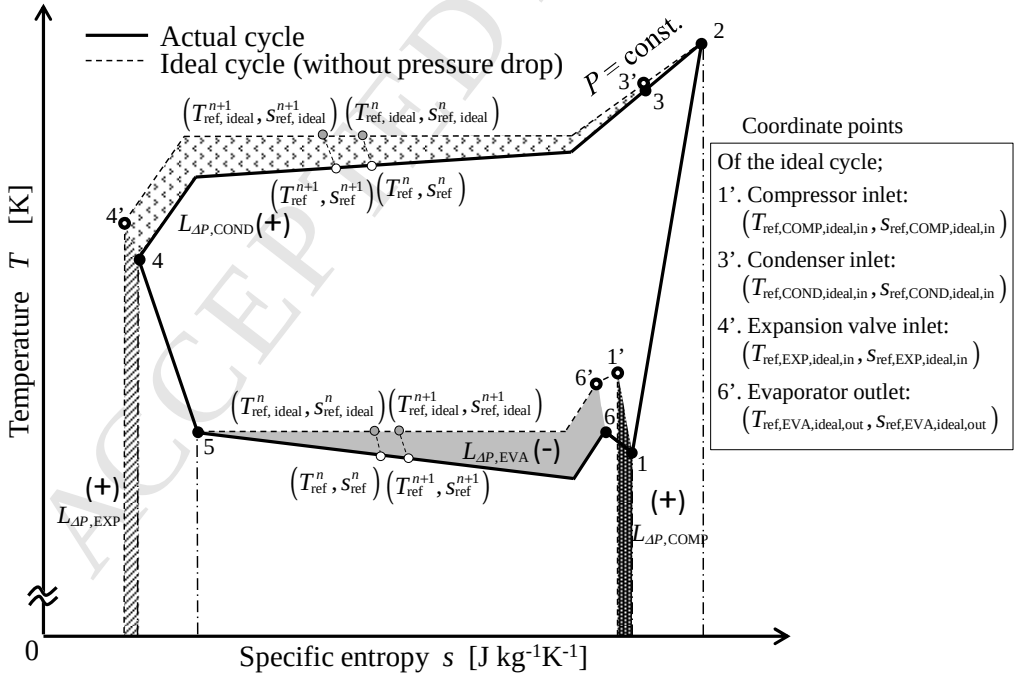

(b) irreversible loss caused by pressure drop

Figure 3 Calculation procedures for irreversible losses

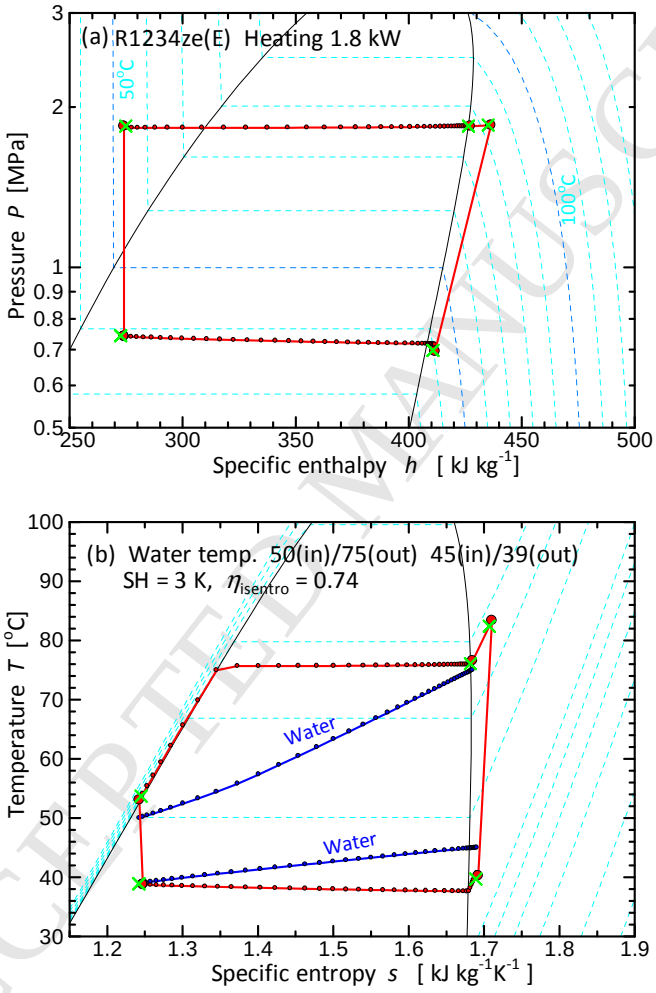

Figure 4 Simulation results for R1234ze(E) at a heating load of 1.8 kW and condensation temperature of 75 °C; the cross and circle symbols represent measured and simulated points, respectively.

(a) P-h diagram (b) T-s diagram

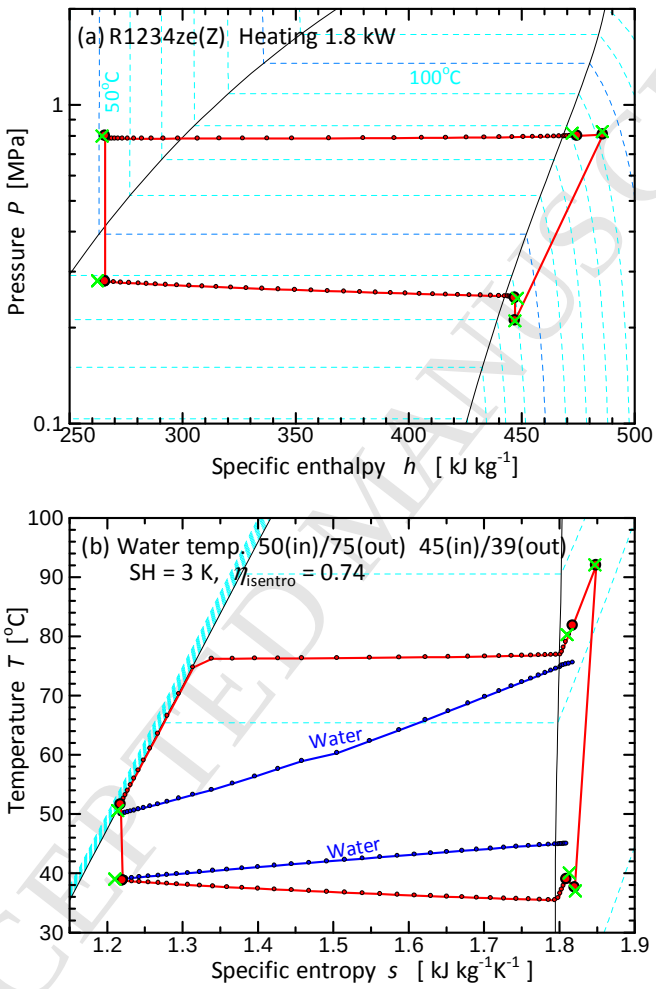

Figure 5 Simulation results for R1234ze(Z) at a heating load of 1.8 kW and condensation temperature of 75 °C; the cross and circle symbols represent measured and simulated points, respectively.

(a) P-h diagram (b) T-s diagram

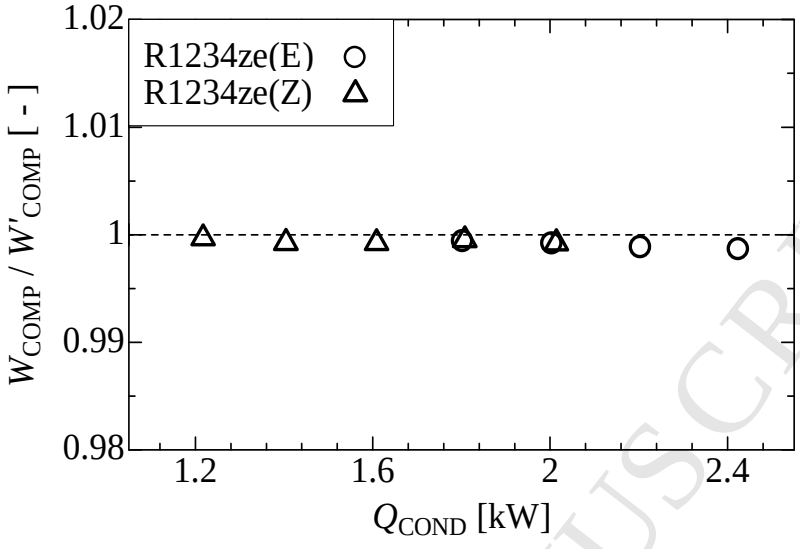

Figure 6 Validation of the data reduction method considering irreversible losses

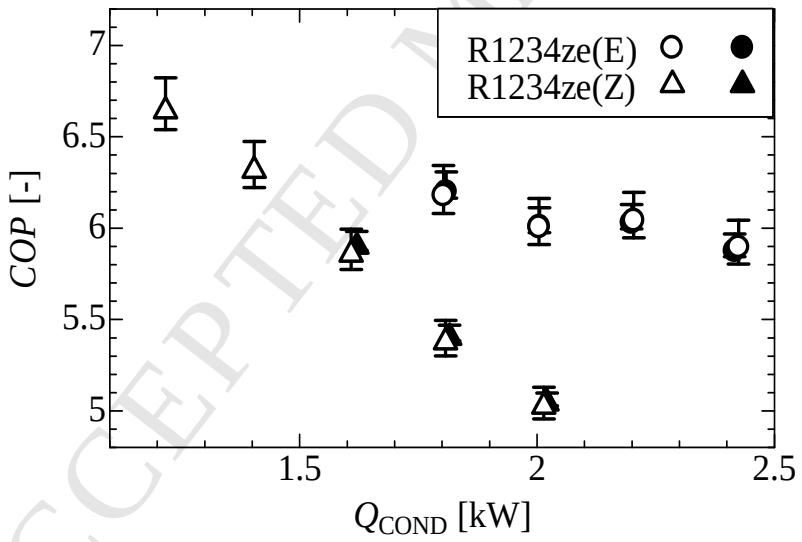

Figure 7 Experimental results of COP and heating load at the optimum charge amount and a condensation temperature of approximately 75 °C (white and black symbols denote COP obtained by refrigerant-side heat balance as Eq. (5a) and water-side heat balance as Eq. (5b), respectively. Vertical bars appended to symbols show the propagated measurement uncertainty specified in Appendix A.)

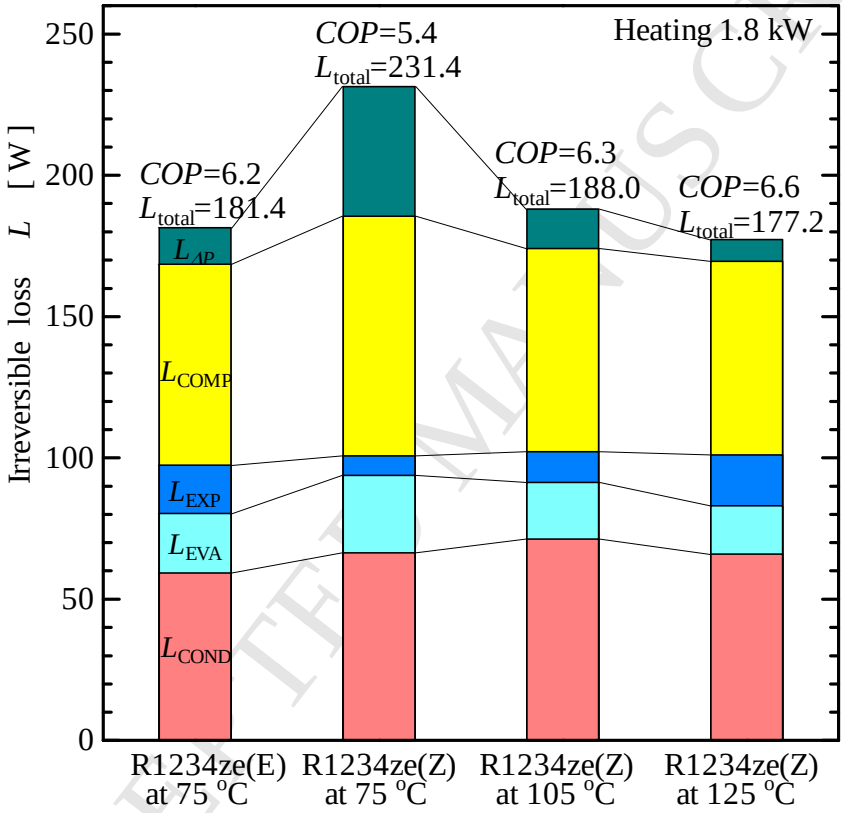

Figure 8 Breakdown of irreversible losses obtained from simple simulations for R1234ze(E) and R1234ze(Z) at the condensation temperatures 75, 105, and 125 °C

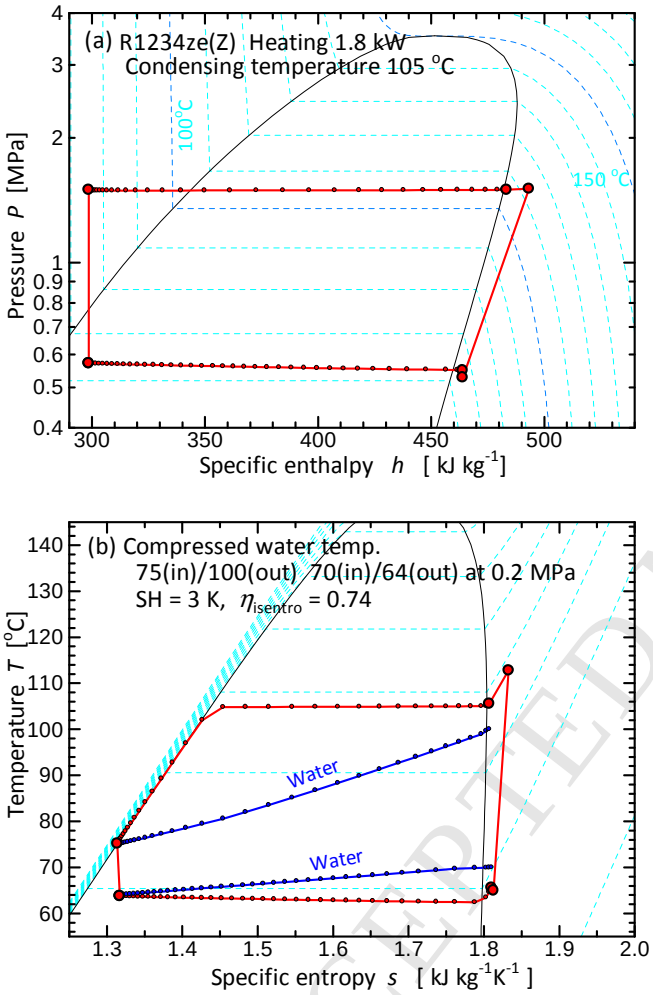

Figure 9 Simulation results for R1234ze(Z) at a condensing temperature of 105 °C

(a) P-h diagram (b) T-s diagram

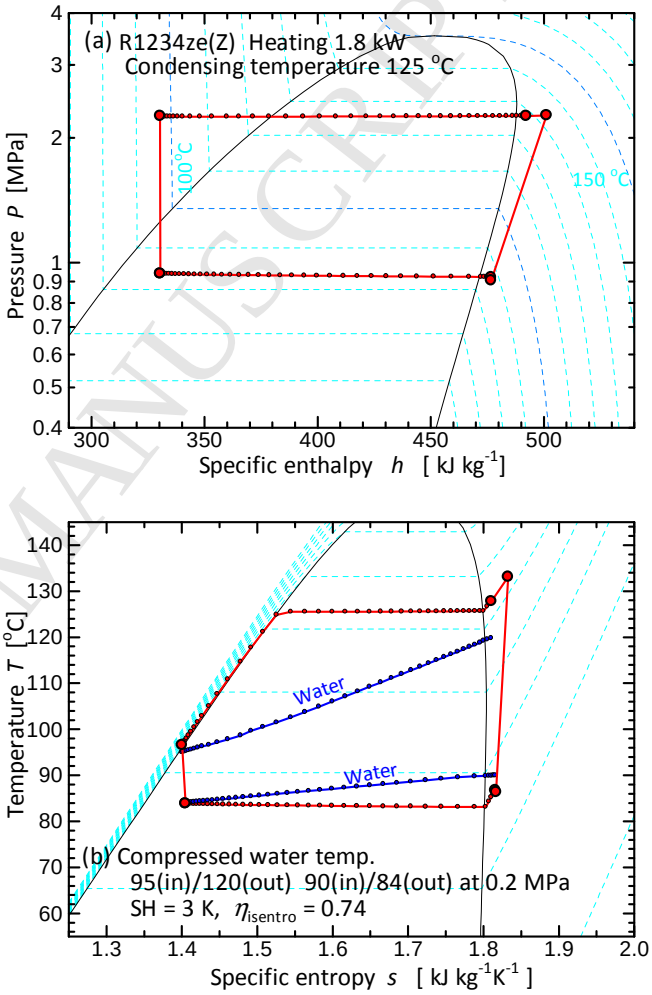

Figure 10 Simulation results for R1234ze(Z) at a condensing temperature of 125 °C

(a) P-h diagram (b) T-s diagram

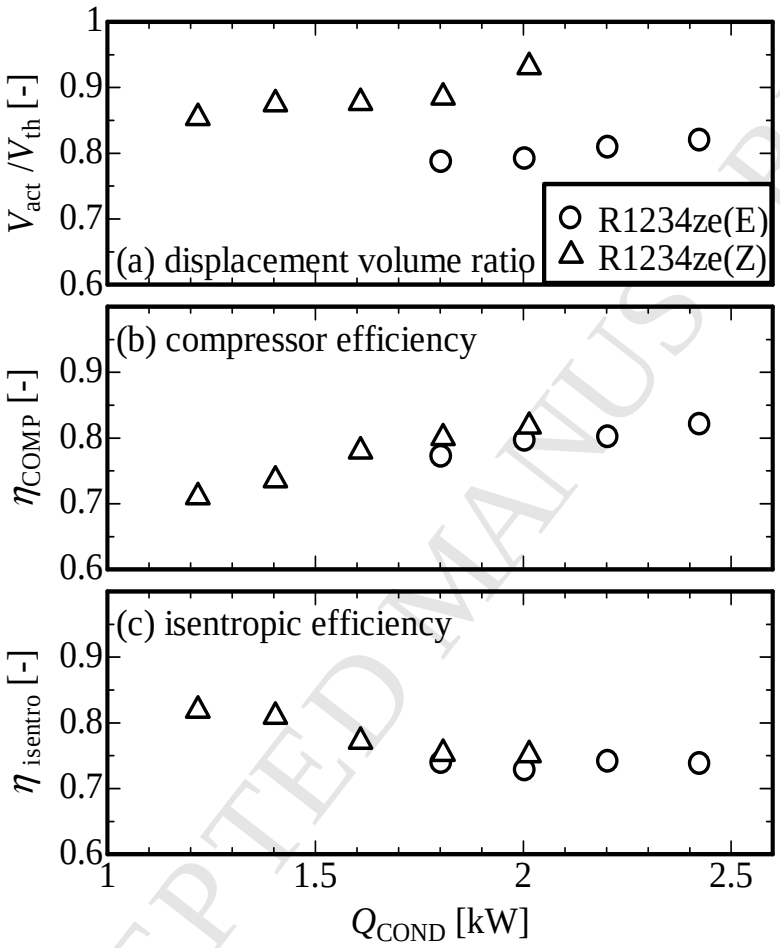

Figure B.1 Change in efficiency of the tested compressor for R1234ze(E) and R1234ze(Z).
(a) volume ratio of the actual displacement to the theoretical displacement (b) compressor efficiency (c) isentropic efficiency

Figure Captions

Figure 1 Results of the thermodynamic assessment assuming an ideal reversed Rankine cycle

(a) theoretical COP (b) volumetric capacity

Figure 2 Experimental apparatus

Figure 3 Calculation procedures for irreversible losses

(a) irreversible losses in main components (b) irreversible loss caused by pressure drop

Figure 4 Simulation results for R1234ze(E) at a heating load of 1.8 kW and condensation temperature of 75 °C; the cross and circle symbols represent measured and simulated points, respectively.

(a) P-h diagram (b) T-s diagram

Figure 5 Simulation results for R1234ze(Z) at a heating load of 1.8 kW and condensation temperature of 75 °C; the cross and circle symbols represent measured and simulated points, respectively.

(a) P-h diagram (b) T-s diagram

Figure 6 Validation of the data reduction method considering irreversible losses

Figure 7 Experimental results of COP and heating load at the optimum charge amount and a condensation temperature of approximately 75 °C (white and black symbols denote COP obtained by refrigerant-side heat

balance as Eq. (5a) and water-side heat balance as Eq. (5b), respectively. Vertical bars appended to symbols show the propagated measurement uncertainty specified in Appendix A.)

Figure 8 Breakdown of irreversible losses obtained from simple simulations for R1234ze(E) and R1234ze(Z) at the condensation temperatures 75, 105, and 125 °C

Figure 9 Simulation results for R1234ze(Z) at a condensing temperature of 105 °C

(a) P-h diagram (b) T-s diagram

Figure 10 Simulation results for R1234ze(Z) at a condensing temperature of 125 °C

(a) P-h diagram (b) T-s diagram

Table 1 Fundamental information for selected refrigerants

		R410A	R134a	R245fa	R1234ze(E)	R1234ze(Z)[*e]
Safety classification[*a]	-	A1	A1	B1	A2L	A2L (expected)
GWP_{100}	-	2088[*b]	1300[*b]	1030[*b]	6[*c]	< 10 (expected)
Critical temperature	[^{o}C]	71.3	101.1	154.0	109.4	150.1
Critical pressure	[MPa]	4.90	4.06	3.65	3.64	3.53
Normal boiling point	[^{o}C]	-51.7	-26.1	15.1	-19.0	9.8
Saturation pressure[*d]	[MPa]	1.88	0.77	0.18	0.58	0.21
Latent heat of vaporization[*d]	[kJ kg^{-1}]	178.3	173.1	187.3	162.9	204.2
Vapor density[*d]	[kg m^{-3}]	76.5	37.5	10.2	30.6	10.3

*a ANSI/ASHRAE Standard 34-2010, including Erratum Appendix B to ANSI/ASHRAE Standard 34-2001 (2004) and Addendum “i” to ANSI/ASHRAE Standard 34-2010 (2011)

*b IPCC 4th report (2007)

*c Honeywell Material Safety Data Sheet (2011)

*d evaluated at 30 °C using Refprop ver. 9.0 (Lemmon et al. 2010)

*e Osafune et al. (2013), Koyama et al. (2012, 2013), Higashi (2013), Akasaka (2013)

Table 2 Calculation conditions for thermodynamic assessment

Isentropic efficiency of compressor	-	1.0
Volumetric efficiency of compressor	-	1.0
Temperature lift (difference between condensation temperature and evaporation temperature)	[K]	35
Degree of subcool	[K]	20
Degree of superheat	[K]	3
Range of condensation temperatures	[K]	30 <

Table 3 Conditions for experiment and simple simulations

			experiment	simulation I	simulation II	simulation III
Water	Heat sink water temperature in condenser	[°C]	50(in) 75(out)	50(in) 75(out)	75(in) 100(out)*	95(in) 120(out)*
	Heat source water temperature in evaporator	[°C]	45(in) 39(out)	45(in) 39(out)	70(in) 64(out)	90(in) 84(out)
Heat transfer rate (i.e., heating load)		[kW]	1.2 to 2.4		1.8	
Degree of superheat at evaporator outlet		[K]		3		
Degree of subcool at condenser outlet		[K]	20 to 25		Resulting	
Compressor	Isentropic efficiency	[-]	0.71 to 0.84		0.74	
	Length of suction pipe	[m]		3		
	Heat loss through discharge pipe	[kW]	0.09 to 0.12		0.1	
Heat exchangers (condenser/evaporator)	Length	[m]		7.2		
	Number of circuits	[-]		1		
	Inner diameter of outer tube	[mm]		13.88		
	Outer diameter of inner tube	[mm]		9.53		
	Inner diameter of inner tube	[mm]	7.53 (Equivalent inner diameter with helical inner-micro-fins)			

* assuming compressed water at 0.2 MPa

Table 4 Applied correlations for simple simulations

Heat exchangers	Refrigerant side	Condenser	Heat transfer coefficient	Cavallini et al. (2009) for two phase zone, and Carnavos (1980) for single phase zone, with the correction method of Kondou and Hrnjak (2012)
			Pressure drop	Goto et al. (2001, 2007) for two phase zone, and Jensen and Vlankancic (1999) for single phase
		Evaporator	Heat transfer coefficient	Mori et al. (2002) for two phase zone, and Carnavos (1980) for single phase zone
			Pressure drop	Kubota et al. (2001) for two phase zone, and Jensen and Vlankancic (1999) for single phase
	Water side	Condenser/ Evaporator	Heat transfer coefficient	Wiegand and Baker (1942)
Compressor	Eqs. (6) and (7)			
Expansion valve	Assuming an isenthalpic process: h = Constant			

Table 5 Comparison of irreversible losses and COP between experiment and simple simulations at a heating load of 1.8 kW (Percentages in parentheses are relative deviations of the simulation results to the experimental results).

	Condensation temperature					
	75 °C				105 °C	125 °C
	R1234ze(E)		R1234ze(Z)		R1234ze(Z)	R1234ze(Z)
	experiment	simulation	experiment	simulation	simulation	simulation
L_{COND}	56.4	59.3 (+5%)	60.4	66.4 (+10%)	71.3	65.9
L_{EVA}	18.3	21.0 (+15%)	22.8	27.4 (+20%)	20.0	17.2
L_{EXP}	16.7	17.1 (2%)	6.1	6.9 (+13%)	10.9	17.9
L_{COMP}	72.0	71.2 (-1%)	77.8	84.8 (+9%)	71.9	68.5
$L_{\Delta P}$	14.1	12.8 (-9%)	52.9	46.0 (-13%)	13.9	7.7
L_{total}	177.5	181.4 (+2%)	220.0	231.4 (+5%)	188.0	177.2
COP	6.2	6.2 (-0%)	6.6	5.4 (-18%)	6.3	6.6

Table A.1 Measurement uncertainties.

measurement points		instrument type, max. reading (model)	uncertainty
refrigerant temperature	$U_{T_{ref}}$	K type thermocouple of ϕ 1.0 mm	±0.05 °C
water temperature	$U_{T_{H2O}}$		
refrigerant flow rate	$U_{m_{ref}}$	Coriolis type mass flow meter, Max. 220 kg h^{-1} (Oval ALTImass, CA003L)	0.22% of reading
water flow rate	$U_{V_{H2O}}$	gear type volumetric flow meter, Max. 300 L h^{-1} (Oval, LGV45A30-G130)	0.5% of reading
refrigerant absolute pressure	U_P	absolute pressure transducer, Max. 5 MPa$_{abs}$ (Kyowa, PHS-50KA)	± 7 kPa
		absolute pressure transducer, Max. 2 MPa$_{abs}$ (Kyowa, PHS-20KA)	± 3.8 kPa
inverter input power	-	digital power meter, Max. 12 kW (Yokogawa, 2533)	0.4% of reading
compressor input power	$U_{W_{COMP}}$	digital power meter, Max. 50 kW (Yokogawa, WT1600)	0.3% of reading

Title:

Low GWP refrigerants R1234ze(E) and R1234ze(Z) for high temperature heat pumps

Authors:
Sho Fukuda, Chieko Kondou, Nobuo Takata, Shigeru Koyama

Highlights

- COP and irreversible loss were evaluated at condensation temperatures above 75 °C.
- Evaluation of pressure drop yielded reasonable assessment of cycle performance for R1234ze(Z).
- At condensation temperature 75 °C, COP of R1234ze(E) was higher than that of R1234ze(Z).
- A numerical approach indicated that R1234ze(Z) is suitable for condensation temperatures above 100 °C.